

Protease-activated receptor 1 knockout reduces experimentally induced liver fibrosis.

Anne Rullier, Jennifer Gillibert-Duplantier, Pierre Costet, Gaëlle Cubel, Valérie Haurie, Cyril Petibois, Danièle Taras, Nathalie Dugot-Senant, Paulette Bioulac-Sage, Jean Rosenbaum

▶ To cite this version:

Anne Rullier, Jennifer Gillibert-Duplantier, Pierre Costet, Gaëlle Cubel, Valérie Haurie, et al.. Protease-activated receptor 1 knockout reduces experimentally induced liver fibrosis.. AJP - Gastrointestinal and Liver Physiology, 2008, 294 (1), pp.G226-35. 10.1152/ajpgi.00444.2007 . inserm-00181396

HAL Id: inserm-00181396 https://inserm.hal.science/inserm-00181396

Submitted on 10 Sep 2009

HAL is a multi-disciplinary open access archive for the deposit and dissemination of scientific research documents, whether they are published or not. The documents may come from teaching and research institutions in France or abroad, or from public or private research centers. L'archive ouverte pluridisciplinaire **HAL**, est destinée au dépôt et à la diffusion de documents scientifiques de niveau recherche, publiés ou non, émanant des établissements d'enseignement et de recherche français ou étrangers, des laboratoires publics ou privés.



Protease-activated receptor 1 (PAR-1) knock-out reduces experimentally-induced liver fibrosis.

Anne Rullier^{1, 2}, Jennifer Gillibert-Duplantier¹, Pierre Costet³, Gaëlle Cubel¹, Valérie Haurie¹, Cyril Petibois⁴, Danièle Taras¹, Nathalie Dugot-Senant¹, Paulette Bioulac-Sage^{1, 2} and Jean Rosenbaum¹.

¹INSERM, U889, Bordeaux, F-33076 France; IFR 66, Université Victor Segalen Bordeaux 2, Bordeaux, F-33076 France

²CHU de Bordeaux, Hôpital Pellegrin, Department of Pathology, Bordeaux, F-33076 France
³Université Victor Segalen Bordeaux 2, Animalerie spécialisée, Bordeaux, F-33076 France
⁴CNRS, UMR5084, Bordeaux, F-33076 France; Université Victor Segalen Bordeaux 2, Bordeaux, F-33076 France.

Key words : liver fibrosis, hemostasis, thrombin, hypoxia, lymphocytes

Running head : PAR-1 knock-out protects against liver fibrosis

Contact information

Jean ROSENBAUM, INSERM U889, Université Victor Segalen Bordeaux 2, 146, Rue Léo Saignat, 33076 Bordeaux, FRANCE

Tel: +33 5 57 57 15 94; Fax: +33 5 56 51 40 77; e-mail: jean.rosenbaum@gref.ubordeaux2.fr

Number of tables : 4, figures : 6.

Abbreviations : alpha smooth muscle actin (ASMA); matrix metalloproteinase (MMP); Protease-Activated Receptor (PAR); carbon tetrachloride (CCl₄,); connective tissue growth factor (CTGF); monocyte chemotactic protein-1 (MCP-1); Fourier Transformed-infrared (FT-IR); Platelet Derived Growth Factor (PDGF)

Abstract

Thrombin inhibition protects against liver fibrosis. However, it is not known whether thrombin profibrogenic effect is due to effects on blood coagulation or to signaling via proteaseactivated receptors (PAR). We took advantage of the lack of blood coagulation defects in PAR-1 knock-out mice. Acute CCl₄ toxicity was similar in wild-type (WT), PAR-1^{-/-} and PAR-1^{+/-} mice as judged by aminotransferases levels, area of liver necrosis, and liver peroxidation measured by Fourier transformed infrared spectroscopy. Fifteen mice/group received CCl₄ or its solvent for 6 weeks (300µl/kg, 3 times a week). Fibrosis area was increased ten-fold by CCl₄ treatment in WT mice. PAR-1 deficiency protected against fibrosis, with a 36% and 56% decrease in PAR-1^{+/-} and PAR-1^{-/-} mice, respectively (p < 0.001). Similar results were obtained for the area of activated fibrogenic cells (64% and 79% decrease in PAR-1^{+/-} and PAR-1^{-/-} mice, respectively, p<0.001). These findings were corroborated by measurements of type I collagen, matrix metalloproteinase-2 and PDGFB-R mRNA levels. There was also a significant decrease in T lymphocyte infiltration in PAR-1-deficient mice. Altogether, these results suggest that thrombin pro-fibrogenic effects are independent of effects on blood coagulation, but are instead due to direct effects on fibrogenic cells and possibly on T lymphocytes.

Key words : liver fibrosis, hemostasis, thrombin, hypoxia, lymphocytes

Introduction

Liver fibrosis is the major complication of most chronic liver diseases leading eventually to cirrhosis and hepatocellular carcinoma. Fibrosis deposition results from the activation of fibrogenic cells, the major ones being hepatic stellate cells and portal fibroblasts (22). Activated fibrogenic cells have a myofibroblastic phenotype characterized notably by the expression of alpha smooth muscle actin (ASMA) and are responsible for a high-level synthesis of extracellular matrix components, particularly collagen 1, and of extracellular matrix remodeling enzymes such as matrix metalloprotease-2 (MMP-2) (2).

Thrombin is a multifunctional serine protease that plays a central role in hemostasis by converting soluble fibrinogen into an insoluble fibrin clot and by promoting platelet aggregation (11). Thrombin has also a cytokine-like activity exerted via specific cell surface receptors called Protease-Activated Receptors (PAR). PARs belong to the seven transmembrane domain G-protein-coupled receptor superfamily. There are altogether four PARs, 3 of them, PAR-1, PAR-3 and PAR-4, being thrombin receptors. All PARs are activated by cleavage of the amino terminal sequence of the extracellular exodomain, resulting in a new amino terminal sequence which acts as a tethered ligand and initiates signal transduction (11). PAR-1 is expressed by several human cellular types like platelets, endothelial cells, fibroblasts, smooth muscle cells and T lymphocytes (12, 14, 34). Besides its procoagulant effects, many studies have shown the implication of thrombin and PAR-1, its main receptor, on inflammation, fibrogenesis and extracellular matrix remodeling in several organs and particularly in kidney and liver. Thus, we and others have shown that PAR-1 was overexpressed in human liver fibrosis (27, 34). In vitro, thrombin via PAR-1 stimulates rat (16, 26) and human (24) hepatic stellate cell proliferation, it regulates their migration (18) and their capacity to synthesize extracellular matrix components (17) and protease inhibitors (30).

Finally, we recently demonstrated that a thrombin antagonist was protective against carbon tetrachloride-induced fibrosis (CCl_4) (15).

The profibrotic effects of thrombin could result from one of two signaling pathways. Activation of hemostasis would result in the occurrence of fibrin deposition and microthrombi in the liver parenchyma (31), leading to hypoxia and subsequent fibrogenesis (10, 37). However, PAR-1 signaling is known to result in the increased expression of a series of extracellular matrix molecules (7, 17) and profibrogenic mediators such as connective tissue growth factor (CTGF) (8) or monocyte chemotactic protein-1 (MCP-1) (26) and could thus account for the pro-fibrogenic effect of thrombin. Fiorucci et al have shown that a PAR-1 antagonist reduced liver fibrosis induced by bile duct ligation (16). These results are in favor of a significant role of PAR-1 signalization in liver fibrogenesis. Indeed, since rodent platelets do not express PAR-1 but instead use PAR-3 together with PAR-4, PAR-1 antagonists do not alter blood coagulation (9) and their protective effects are thus the consequence of the blockage of PAR-1 function in other cells such as fibro/myofibroblasts. However, the use of pharmacological antagonists may lead to improper results because of incomplete effects on one hand, or of non specific effects on the other (13).

Thus, in this study, we used mice where PAR-1 expression was abolished via homologous recombination in order to clarify the implication of PAR-1 in liver fibrogenesis.

Material and Methods

<u>Animals</u>

PAR-1-deficient mice were established by Connolly et al (9) and were studied in the C57BL/6 background. We used only male animals, aged 10-12 weeks, and weighing 31.0 ± 2.5 g at the onset of the study. The mice were allowed food and water ad libitum, and were housed at a constant temperature with a 12-h light/dark cycle during the study. Genotyping was performed using tail blood sample spotted onto Flinders Technology Associates (FTA) filter paper (Whatman, Oxon, UK) that was processed according to instructions from the manufacturer. Primers PAR-1s (5'-GGA GAA AAA TGA AAG CGT CCT GC) and PAR-1as (5'-AGC CTT GCA TCA GGT TCT CAC TG) were used to amplify a 660 bp product from the wild type allele whereas primer PAR-1as neo (5'-TGA GAC GTG CTA CTT CCA TTT GTC AC) in combination with PAR-1s were used to amplify a 400 bp product from the targeted allele. Fragments were amplified using Hot start polymerase (Qiagen, Venlo, The Netherlands) with a PCR buffer containing 1.5 mM MgCl₂ in a final volume of 50µl under the following conditions : 94°C, 1 min, 61.9°C, 1 min, 72°C, 1 min for 35 cycles. PCR products were visualized by electrophoresis on 1.5% agarose gels containing ethidium bromide. Knock-out, heterozygous and paired littermates wild-type animals were used. This study was performed in accordance with the European Community Standards on the Care and Use of Laboratory Animals and approved by the Animal Care and Use Committee of the University of Bordeaux 2.

Carbon tetrachloride-induced liver lesions

CCl₄.acute liver toxicity

To assess the necrotic and inflammatory changes caused by acute exposure to CCl₄ (Sigma, St Quentin-Fallavier, France), a single intraperitoneal injection of 300µl/kg (in olive oil) was

administered to PAR-1^{+/+}, PAR-1^{+/-} and PAR-1^{-/-} mice (5 mice/group). Mice without any treatment were used as controls. Blood and liver samples were obtained after 48 hours. Liver tissue was snap-frozen or fixed in 10% neutral formalin. Sera were collected for biochemical analysis.

*CCl*₄*-induced liver fibrosis*

Liver fibrosis was induced by the intraperitoneal injection of 300µl/kg body weight CCl₄ mixed with olive oil three times weekly for 6 weeks. Four groups of mice were studied : three groups received CCl₄ (group 1 : PAR-1^{+/+} mice, group 2 : PAR-1^{+/-} mice, group 3 : PAR-1^{-/-} mice; 15 animals per group), whereas one control group of PAR-1^{+/+} mice received only the CCl₄. solvent (n=6). Mice were sacrificed after 6 weeks of treatment, 2 days following the last injection. Blood and sera were collected. Liver samples were harvested, weighted and rapidly sliced: sections from several lobes were fixed in 10% neutral formalin for histological examination; other parts were snap frozen in liquid nitrogen for RNA extraction or Western blot. Spleen weight was also measured.

Measure of CCl₄ acute liver toxicity

Acute liver toxicity was assessed by three different methods in a blinded fashion. First, we tested the levels of serum aminotransferases on an automated analyser in the Biochemistry Department of Pellegrin Hospital in Bordeaux. Secondly, we analyzed the extent of liver peroxidation induced by CCl_4 in microsomal fractions of mouse liver by Fourier Transformed-infrared (FT-IR) spectroscopy as previously described (29). Ward's algorithm was used on OPUS 4.0 software (Bruker, Ettlingen, Germany) for spectra classification on the spectral interval that are the most representative of the v(C-O) sugar absorptions (1130-930 cm⁻¹).

Third, the area of centrolobular necrosis was measured using a histomorphometric method based on hemalun-eosin and saffron stained slides. Slides were examined with a Zeiss Axioplan 2 microscope (Carl Zeiss Microscopy, Jena, Germany). Images were acquired with an AxioCam camera (Carl Zeiss Vision, Hallbergmoos, Germany) by means of the Axiovision image processing and analysis system (Carl Zeiss Vision) and quantitative data were obtained using a computerized image analysis (KS300, Carl Zeiss Vision). Sampling corresponded to three sections randomly taken from left, median and right major lobes. Analysis was performed on an average of ten fields per sample randomly taken using the x10 objective. Necrosis was expressed as a percentage of necrotic area on the total surface of liver analyzed.

Fibrosis assessment

Four μ m thick sections from formalin fixed paraffin embedded liver tissue were prepared and stained with picrosirius red (saturated picric acid in distillated water containing 0.1% (w/v) picrosirius red F3B (BDH Chemicals Ltd., Poole, UK) to allow visualization of liver fibrosis. Sections were mounted with Eukitt (O Klinder GmbH and Co, Freiburg, Germany) before examination. The analysis was performed on the whole surface of the sample, including three sections randomly taken from left, median and right major lobes using the x 4 objective of a Coolscope microscope (Nikon, Champigny sur Marne, France) and the Lucia version 5.0 software (Nikon) in a blinded fashion. Large centrolobular veins (diameter >150 μ m) and large portal tracts were excluded. Fibrosis deposition was expressed as a percentage of picrosirius red stained area on the total area of the sample.

Immunolabelling for ASMA was performed on serial sections of formalin fixed paraffin embedded liver tissue with a monoclonal antibody (Dako A/S, Glostrup, Denmark, clone 1A4) diluted to 1/400, after heat induced antigen retrieval (citrate buffer pH 6, ten minutes). The signal was amplified by EnVision^{TM+} dextran polymer (Dako A/S) and revealed with liquid diaminobenzidine substrate (Dako A/S). Results were analyzed with the same histomorphometric method using the x 20 objective.

Real-time quantitative RT-PCR

Total RNA was extracted from liver samples using the Nucleospin RNA II (Macherey Nagel, Düren, Germany). The quality of the total RNA samples were determined by electrophoresis through agarose gels and staining with ethidium bromide, and the 18S and 28S RNA bands were visualized under UV light. RNA was reverse transcribed using Superscript II (Promega, Charbonnières-les-Bains, France). Nucleotide sequences of primers for collagen $\alpha 1(I)$, MMP-2, Platelet Derived Growth Factor (PDGF) β receptor, MCP-1, CTGF and PAR-1 target genes, and for RLP0 (encoding the human acidic ribosomal phosphoprotein P0, used as a control) are shown in Table 1. No template and no-reverse transcriptase were also performed as controls.

All PCR reactions were performed using a Stratagene X4000 thermocycler (Stratagene, Amsterdam, The Netherlands) and the SYBR Green PCR Core reagents kit (Bio-Rad, Marnes-la-Coquette, France). Five microliters of diluted complementary DNA samples (produced from 3ng total RNA) was added to 20µl of the PCR master mix. The thermal cycling conditions comprised an initial denaturation step at 95°C for 10 minutes and 45 cycles at 95°C for 15 seconds and 65°C for 1 minute. Experiments were performed with duplicates for each data point. Each sample was normalized on the basis of its expression of the RLPO gene as previously described (4). All amplified sequences were also verified by sequencing in a ABI prism 3130 xl Genetic Analyser (HITACHI High Technologies Corporation, Tokyo, Japan). In order to compare quantitative values from one sample to another, the relative expression of each gene was also normalized to the sample displaying the smallest amount of

RNA and called calibrator. Each sample-normalized value was divided by the calibratornormalized value to give the final relative expression level.

Hypoxia assessment

To detect liver hypoxic areas, an intraperitoneal injection of 60mg/kg pimonidazole (HypoxyprobeTM-1 kit, Chemicon International, Temecula, CA) was performed one hour before sacrifice. Pimonidazole is a stable and aqueous soluble molecule that specifically forms adducts in hypoxic cells. Such adducts are stable on time and can be detected by a specific monoclonal antibody called Hypoxyprobe 1-Mab-1 on formalin-fixed paraffin embedded tissues. The signal was detected according to the manufacturer's procedure. Briefly, after inhibition of endogenous peroxidase, sections were incubated with 0.01% Pronase during 40 min at 40°C and then with Dako blocking system during 5 min at room temperature before incubation with Hypoxyprobe 1-Mab-1 (1/50) 45 min at room temperature. After washing, sections were incubated with biotin-SP-conjugated F(ab')2 fragment of a rabbit anti-mouse IgG. The signal was detected after application of peroxidase conjugated streptavidin followed by liquid diaminobenzidine substrate. Positive hepatocytes were counted using a Coolscope microscope (Nikon) in twelve non overlapping fields at the x 20 objective.

Assessment of T lymphocyte infiltration

In order to study T lymphocyte infiltration, we used an immunohistochemical method with a polyclonal CD3 antibody (Dako A/S) diluted to 1/100, after heat induced antigen retrieval (citrate buffer pH 6, ten minutes). The staining was amplified as described above. Centrolobular CD3-positive lymphocytes were counted in twelve fields at the 40 objective using the Coolscope microscope.

MMP-2 immunoblots

Sixteen micrometers cryostat sections were solubilized in 25 μ l 10% glycerol, 1% SDS at room temperature for 15 min. Protein concentration was estimated from A₂₈₀ readings. Samples normalized for protein concentration were separated on 10% SDS-PAGE gels, transferred to polyvinylidene difluoride membranes. The blots were incubated with a MMP-2 antibody from Santa Cruz Biotechnologies (sc-13594, Santa Cruz, CA) and the signals were detected with enhanced chemiluminescence.

Statistical analysis

All data were expressed as median (range). Kruskal-Wallis test was performed to compare groups. Results were considered to be significant when p<0.05.

Results

Genotyping

About only 7% of mice born from crossing between PAR-1^{+/-} mice were PAR-1^{-/-} males. This sub-Mendelian ratio is in accordance with previous publications (9) and is due to a roughly 50% embryonic lethality of PAR-1^{-/-} mice resulting from hemorrhage and cardiovascular failure at midgestation because of an abnormal endothelial function (19).

<u>CCl₄-acute liver toxicity</u>

Since CCl_4 -induced fibrosis is under the dependence on CCl_4 ability to induce liver necrosis and inflammation, we took great care to ensure that all 3 groups of mice had a similar response to an acute CCl_4 challenge. No mice died during this experiment. Serum aminotransferase levels were very high in animals receiving CCl_4 (Table 2). There was however no significant difference between PAR-1^{+/+}, PAR-1^{+/-} and PAR-1^{-/-} mice. Similarly, PAR-1^{+/-} and PAR-1^{-/-} mice did not differ from PAR-1^{+/+} mice regarding the extent of centrolobular necrosis (Table 2). Finally, we used FT-IR spectroscopy to provide a global analysis of liver peroxidation level induced by CCl₄ in microsomal fractions of mouse liver. Using Ward's algorithm for spectra classification (classification is represented in dendrogram), this allowed a clear discrimination between controls and CCl₄-treated animals, although the 3 treated groups clustered together (Fig 1). We also measured liver infiltration by CD3-positive lymphocytes. Median value was 49.0 (range : 32-95) in control untreated mice, and 52.5 (47-73), 38.0 (36-59) and 45.0 (39-48) for PAR-1^{+/+}, PAR-1^{+/-} and PAR-1^{-/-}mice treated with CCl₄, respectively. These values did not differ significantly between them (p = 0.07 by ANOVA).

CCl₄-induced liver fibrosis

Vital parameters and liver function tests

During CCl₄ treatment, three PAR-1^{+/+} mice and one PAR-1^{-/-} mouse died; the difference of mortality was not statistically different between the three groups. After six weeks of CCl₄ treatment, mouse body weight and spleen weight were not different between the four groups (controls, PAR-1^{+/+}, PAR-1^{+/-} and PAR-1^{-/-} treated mice) whereas liver weight and consequently liver weight to body weight ratio were significantly higher in all CCl₄ treated groups as compared to controls (Table 3); these 3 groups were however not different from each other. Treatment with CCl₄ also resulted in increased values of serum transaminases with no difference between the three groups (Table 3).

PAR-1 expression

PAR-1 expression was measured with real-time PCR in the livers of PAR-1^{+/+} control animals or those that received CCl₄ for 6 weeks. The median PAR-1/RLP0 value in controls was 6802 (range : 2481-12916), whereas it was 13372 in CCl₄-treated animals (range : 9455-22256). The difference was highly significant (p = 0.008), in accordance with previous data (16).

Fibrosis measurement

CCl₄ treatment induced fibrosis deposition predominantly located in centrolobular areas. The area of fibrosis increased by about tenfold from 0.25 (0.13-0.35) % of field area in control group which received only olive oil, to 2.31 (1.79-3.20) % in CCl₄-treated PAR-1^{+/+} mice. The area of fibrosis was decreased by 56% in PAR-1^{-/-} mice (1.16%; 0.88-1.44) and by 36% (1.58%; 1.16-2.80) in PAR-1^{+/-} mice as compared to PAR-1^{+/+} mice (p<0.001) (Fig 2).

ASMA staining was restricted to vessel walls in control group whereas in CCl₄ treated groups ASMA-positive cells were observed around the centrolobular areas and infiltrated the lobule. The area of ASMA-positive cells increased by tenfold from 0.25 (0.21-0.37) % in control group, to 2.69 (1.58-3.76) in CCl₄ PAR-1^{+/+} mice. The area of ASMA-positive cells was decreased by 79% in PAR-1^{-/-} mice (0.76%; 0.50-1.73) and by 64% (1.14%; 0.97-1.62) in PAR-1^{+/-} mice as compared to PAR-1^{+/+} mice (p<0.001) (Fig 3).

Expression of fibrosis-related molecules

We evaluated the mRNA levels of collagen $\alpha 1(I)$, a major component of liver fibrosis, PDGF β -R, a marker of fibrogenic cell activation, and MMP-2, implicated in extracellular matrix remodeling, using real-time quantitative RT-PCR. The median collagen $\alpha 1(I)/RLP0$ ratio was 2.25 (1-14) in control group whereas it reached 59.5 (18.80-233.20) in PAR-1^{+/+}

mice treated for 6 weeks with CCl_4 . As shown on Fig 4a, PAR-1^{-/-} mice had a significantly lower expression of collagen $\alpha 1(I)$ transcripts, whereas PAR-1^{+/-} mice showed intermediate levels (p=0.008). The median PDGFβ-R/RLP0 ratio was also increased from 1.50 (1-10.70) in the control group to 10.50 (2.80-38.90) in PAR-1^{+/+} mice treated for 6 weeks with CCl₄. There was a trend towards a decrease in PAR-1^{-/-} mice and PAR-1^{+/-} mice although the difference did not reach statistical difference (p=0.063) (Fig 4b). The median MMP-2/RLP0 ratio was 1.60 (1-18.70) in control group whereas it was 64.45 (17-179) in PAR-1^{+/+} mice treated for 6 weeks with CCl₄. As for collagen $\alpha 1(I)$, PAR-1^{-/-} mice had a significantly lower expression of MMP-2 transcripts, whereas PAR-1^{+/-} mice showed intermediate levels (p=0.004) (Fig 4c). MMP-2 expression was also analyzed in a subset of samples using western blot. As shown on Fig. 4d, MMP-2 expression was as expected increased in CCl₄treated PAR-1^{+/+} mice as compared with controls; the increase was abolished in PAR-1^{-/-} mice. Finally, we also assessed the expression of two cytokine genes known to be PAR-1 targets and relevant in the context of liver fibrosis, CTGF (8) and MCP-1 (26). The expression of both genes was increased in CCl₄-treated PAR-1^{+/+} mice as compared to controls, although modestly. In both cases, there was a decrease in PAR-1^{-/-} mice, but it failed to reach statistical significance (Table 4).

Hypoxia

Fig. 5 illustrates hypoxia staining in the different groups of animals. As previously described (10), the staining was localized preferentially in the cytoplasm of centrolobular hepatocytes. Quantitative analysis of all samples demonstrated that the median number of hypoxic hepatocytes was different between the four groups (Fig. 5, p<0.001). The median number of hypoxic hepatocytes was 117.0 (86.0-186.0) in control group whereas it increased to 179.0

(67.0-231.0) in PAR-1^{+/+} mice treated for 6 weeks with CCl₄ (p=0.049). In PAR-1^{-/-} mice, it was down to control level (97.5; 62.0-145.0) (p=0.001). However, the difference was not statistically different between PAR-1^{+/-} mice (162.0; 100.0-201.0) and PAR-1^{+/+} mice.

T lymphocyte infiltration

Fig. 6 illustrates CD3 staining in the different groups of animals. Quantitative analysis of all samples demonstrated that the median number of CD3-positive lymphocytes was different between the 4 groups (Fig. 6, p<0.001). The median number of CD3-positive lymphocytes was 49.0 (32.0-95.0) in control group whereas it reached 178.5 (146.0-210.0) in PAR-1^{+/+} mice treated for 6 weeks with CCl₄. The number of these cells decreased by 70% (87.5; 66.0-125.0) in PAR-1^{-/-} mice and by 35% (130.0; 98.0-179.0) in PAR-1^{+/-} mice.

Discussion

In this work, we studied the impact of PAR-1 deficiency on mouse liver fibrogenesis in the CCl_4 model. We observed that PAR-1 complete deficiency led to a 56% decrease in the area of fibrosis and almost 80% reduction in the area of ASMA-positive cells. This was paralleled by decreased levels of collagen 1, MMP-2, PDGFβ-R, CTGF and MCP-1 transcripts. These data indicate that PAR-1 deficiency afforded a significant protection against liver fibrosis. Animals with a single deleted allele had an intermediate protection. In addition, we found that PAR-1^{-/-} mice had a significant reduction in the number of hypoxic hepatocytes. It is likely that this reduced hypoxia is the consequence of decreased fibrogenesis, that will improve oxygen supply (21). In turn, since hypoxia is a contributing factor to fibrogenesis (1, 10), its decrease will contribute to the reduction in liver fibrosis.

CCl₄ toxicity results from the liver microsomal metabolism of CCl₄ leading to the generation of the toxic trichloromethyl radical that induce hepatocyte necrosis and apoptosis (32). This results in local inflammation that subsequently triggers fibrogenic cell activation. Since CCl₄ metabolism can be altered by a variety of environmental or genetic mechanisms, we took great care to ensure that CCl₄ toxicity was not altered in the different mouse genotypes under study. We found that PAR-1^{+/+}, PAR-1^{+/-} and PAR-1^{-/-} behaved similarly in response to CCl₄ regarding serum aminotransferases, and the extent of liver necrosis as quantified by histomorphometry. There was also no difference in the number of T lymphocytes infiltrating the parenchyma following an acute lesion, although this infiltration was low in every group at the time point studied. We also used the recently developed method of FT-IR spectroscopy that allows a global assessment of many biochemical parameters in the liver (29) and found again no difference between the 3 experimental groups. Thus, it is likely that the differences we found on fibrosis and ASMA scores truly reflect the role of PAR-1 on fibrogenesis,

although our data do not allow to formally exclude the possibility of a defect in tissue repair mechanisms in PAR-1-deficient mice.

Our results confirm and extend the observations of Fiorucci et al. These authors have found that a synthetic PAR-1 antagonist protected against liver fibrosis in the bile duct ligation model in rats (16). Our own study adds several new pieces of information. First, it strongly suggests that PAR-1 may be a generic mediator of fibrogenesis since it is involved in liver fibrosis resulting from very different mechanisms and involving distinct populations of fibrogenic cells. Indeed, CCl₄-induced fibrosis is a highly inflammatory disease where the main cellular actor is the hepatic stellate cell; on the other hand, bile duct-induced fibrosis is very little inflammatory, and the main cell type responsible for fibrosis deposition is the portal fibroblast (3, 36). Secondly, the use of knock-out animals in our study allows to unambiguously ascribe a pro-fibrogenic role to PAR-1 whereas studies with pharmacological antagonists may lead to improper results because of insufficient specificity of the molecules (13).

As pointed out earlier, an unresolved question is whether the reported liver pro-fibrogenic effects of thrombin are due to its pro-coagulant effect, or to its documented pro-fibrogenic signaling via PAR receptors (17, 24, 27). Our study allows to answer this question. Indeed, mouse platelets do not express PAR-1, but instead use PAR-3 and PAR-4 to respond to thrombin. Thus PAR-1 depletion does not affect thrombin effect on platelets and altogether has no effect on blood coagulation (9). We can thus conclude that the pro-fibrogenic effect of thrombin is largely independent on blood coagulation but instead relies on its ability to activate PAR-1. This is also supported by data from Fiorucci et al (16).

In addition to the direct effects of thrombin on fibrogenic cells, our results point to the possible role of T lymphocytes. T lymphocytes are now acknowledged as key contributors to

liver fibrosis (35). We found that PAR-1 deficient animals had a significantly reduced infiltration of the liver with T lymphocytes. Since the expression of PAR-1 on T lymphocytes is well documented (25, 34) and since thrombin can elicit activation signals in T cells (20, 25), we suggest that PAR-1 deficiency may reduce T lymphocyte accumulation in the liver which may participate in the decreased fibrogenic process.

Since PAR-1 can also be activated by other ligands, such as activated protein C (APC) (33) or MMP-1 (5), it could be argued that the effects of PAR-1 depletion may not reflect only a defect in thrombin signaling. However, APC generation is under the dependence of thrombin, and given that thrombin affinity for PAR-1 is much higher than that of APC, the available concentrations of APC may be insufficient to activate PAR-1 (23). Regarding MMP-1, it is expressed at low levels in the liver and is not upregulated in the course of fibrosis. On the other hand, there is evidence that thrombin is generated in fibrotic liver, as evidenced by the presence of fibrin deposition in experimental (31) or human disease (28). Thus, although the role of alternative PAR-1 ligands can not be completely excluded, most evidence points to thrombin as being the active PAR-1 ligand in this setting.

In conclusion, we have shown that invalidation of PAR-1 induces a significant protection against liver fibrosis. These observations confirm and extend previous data obtained in the bile duct ligation model with a PAR-1 antagonist (16). Thus, altogether, these data suggest that PAR-1 antagonists may be useful in the clinical management of liver fibrosis. This is especially appealing, since contrary to direct thrombin inhibitors, PAR-1 antagonists do not provoke a bleeding risk, and there is moreover great hope that orally active molecules will be available (reviewed in (6)). Finally, the fact that deletion of a single PAR-1 allele was enough

to offer a very significant protection, suggests that complete blockage of PAR-1 function may not be required for a therapeutic effect.

Acknowledgments

We thank Shaun Coughlin for the PAR-1 KO mice, Ivan Bièche for his help in setting up the real-time PCR experiments, and the Biochemistry Department of Pellegrin Hospital, Bordeaux, for performing liver function tests.

References

1. Ankoma-Sey V, Wang Y, and Dai Z. Hypoxic stimulation of vascular endothelial growth factor expression in activated rat hepatic stellate cells. *Hepatology* 31: 141-148, 2000.

2. Arthur MJ, Stanley A, Iredale JP, Rafferty JA, Hembry RM, and Friedman SL. Secretion of 72 kDa type IV collagenase/gelatinase by cultured human lipocytes. Analysis of gene expression, protein synthesis and proteinase activity. *Biochem J* 287 (Pt 3): 701-707, 1992.

3. Beaussier M, Wendum D, Schiffer E, Dumont S, Rey C, Lienhart A, and Housset C. Prominent contribution of portal mesenchymal cells to liver fibrosis in ischemic and obstructive cholestatic injuries. *Lab Invest* 87: 292-303, 2007.

4. **Bieche I, Nogues C, Paradis V, Olivi M, Bedossa P, Lidereau R, and Vidaud M.** Quantitation of hTERT gene expression in sporadic breast tumors with a real-time reverse transcription-polymerase chain reaction assay. *Clin Cancer Res* 6: 452-459, 2000.

5. **Boire A, Covic L, Agarwal A, Jacques S, Sherifi S, and Kuliopulos A.** PAR1 is a matrix metalloprotease-1 receptor that promotes invasion and tumorigenesis of breast cancer cells. *Cell* 120: 303-313, 2005.

6. **Chackalamannil S.** Thrombin receptor (protease activated receptor-1) antagonists as potent antithrombotic agents with strong antiplatelet effects. *J Med Chem* 49: 5389-5403, 2006.

7. Chambers RC, Dabbagh K, McAnulty RJ, Gray AJ, Blanc-Brude OP, and Laurent GJ. Thrombin stimulates fibroblast procollagen production via proteolytic activation of protease-activated receptor 1. *Biochem J* 333 (Pt 1): 121-127, 1998.

8. Chambers RC, Leoni P, Blanc-Brude OP, Wembridge DE, and Laurent GJ. Thrombin is a potent inducer of connective tissue growth factor production via proteolytic activation of protease-activated receptor-1. *J Biol Chem* 275: 35584-35591, 2000.

9. **Connolly AJ, Ishihara H, Kahn ML, Farese RV, Jr., and Coughlin SR.** Role of the thrombin receptor in development and evidence for a second receptor. *Nature* 381: 516-519, 1996.

10. Corpechot C, Barbu V, Wendum D, Kinnman N, Rey C, Poupon R, Housset C, and Rosmorduc O. Hypoxia-induced VEGF and collagen I expressions are associated with angiogenesis and fibrogenesis in experimental cirrhosis. *Hepatology* 35: 1010-1021, 2002.

11. **Coughlin SR.** Thrombin signalling and protease-activated receptors. *Nature* 407: 258-264, 2000.

12. **D'Andrea MR, Saban MR, Nguyen NB, Andrade-Gordon P, and Saban R.** Expression of protease-activated receptor-1, -2, -3, and -4 in control and experimentally inflamed mouse bladder. *Am J Pathol* 162: 907-923, 2003.

13. Di Serio C, Pellerito S, Duarte M, Massi D, Naldini A, Cirino G, Prudovsky I, Santucci M, Geppetti P, Marchionni N, Masotti G, and Tarantini F. Protease-Activated Receptor 1-Selective Antagonist SCH79797 Inhibits Cell Proliferation and Induces Apoptosis by a Protease-Activated Receptor 1-Independent Mechanism. *Basic Clin Pharmacol Toxicol* 101: 63-69, 2007.

14. **Dugina TN, Kiseleva EV, Chistov IV, Umarova BA, and Strukova SM.** Receptors of the PAR family as a link between blood coagulation and inflammation. *Biochemistry* (*Mosc*) 67: 65-74, 2002.

15. Duplantier JG, Dubuisson L, Senant N, Freyburger G, Laurendeau I, Herbert JM, Desmouliere A, and Rosenbaum J. A role for thrombin in liver fibrosis. *Gut* 53: 1682-1687, 2004.

16. Fiorucci S, Antonelli E, Distrutti E, Severino B, Fiorentina R, Baldoni M, Caliendo G, Santagada V, Morelli A, and Cirino G. PAR1 antagonism protects against

experimental liver fibrosis. Role of proteinase receptors in stellate cell activation. *Hepatology* 39: 365-375, 2004.

17. Gaca MD, Zhou X, and Benyon RC. Regulation of hepatic stellate cell proliferation and collagen synthesis by proteinase-activated receptors. *J Hepatol* 36: 362-369, 2002.

18. **Gillibert-Duplantier J, Neaud V, Blanc JF, Bioulac-Sage P, and Rosenbaum J.** Thrombin inhibits migration of human hepatic myofibroblasts. *Am J Physiol Gastrointest Liver Physiol* 293: G128-136, 2007.

19. Griffin CT, Srinivasan Y, Zheng YW, Huang W, and Coughlin SR. A role for thrombin receptor signaling in endothelial cells during embryonic development. *Science* 293: 1666-1670., 2001.

20. Joyce DE, Chen Y, Erger RA, Koretzky GA, and Lentz SR. Functional interactions between the thrombin receptor and the T-cell antigen receptor in human T-cell lines. *Blood* 90: 1893-1901, 1997.

21. Le Couteur DG, Cogger VC, Markus AM, Harvey PJ, Yin ZL, Ansselin AD, and McLean AJ. Pseudocapillarization and associated energy limitation in the aged rat liver. *Hepatology* 33: 537-543, 2001.

22. Lotersztajn S, Julien B, Teixeira-Clerc F, Grenard P, and Mallat A. Hepatic fibrosis: molecular mechanisms and drug targets. *Annu Rev Pharmacol Toxicol* 45: 605-628, 2005.

23. Ludeman MJ, Kataoka H, Srinivasan Y, Esmon NL, Esmon CT, and Coughlin SR. PAR1 cleavage and signaling in response to activated protein C and thrombin. *J Biol Chem* 280: 13122-13128, 2005.

24. Mallat A, Gallois C, Tao J, Habib A, Maclouf J, Mavier P, Preaux AM, and Lotersztajn S. Platelet-derived growth factor-BB and thrombin generate positive and negative signals for human hepatic stellate cell proliferation. Role of a prostaglandin/cyclic AMP pathway and cross-talk with endothelin receptors. *J Biol Chem* 273: 27300-27305, 1998.

25. Mari B, Imbert V, Belhacene N, Far DF, Peyron JF, Pouyssegur J, Van Obberghen-Schilling E, Rossi B, and Auberger P. Thrombin and thrombin receptor agonist peptide induce early events of T cell activation and synergize with TCR cross-linking for CD69 expression and interleukin 2 production. *J Biol Chem* 269: 8517-8523, 1994.

26. Marra F, Arrighi MC, Fazi M, Caligiuri A, Pinzani M, Romanelli RG, Efsen E, Laffi G, and Gentilini P. Extracellular signal-regulated kinase activation differentially regulates platelet-derived growth factor's actions in hepatic stellate cells, and is induced by in vivo liver injury in the rat. *Hepatology* 30: 951-958, 1999.

27. Marra F, DeFranco R, Grappone C, Milani S, Pinzani M, Pellegrini G, Laffi G, and Gentilini P. Expression of the thrombin receptor in human liver: up-regulation during acute and chronic injury. *Hepatology* 27: 462-471, 1998.

28. Marsden PA, Ning Q, Fung LS, Luo X, Chen Y, Mendicino M, Ghanekar A, Scott JA, Miller T, Chan CW, Chan MW, He W, Gorczynski RM, Grant DR, Clark DA, Phillips MJ, and Levy GA. The Fgl2/fibroleukin prothrombinase contributes to immunologically mediated thrombosis in experimental and human viral hepatitis. *J Clin Invest* 112: 58-66, 2003.

29. Melin AM, Perromat A, and Deleris G. Pharmacologic application of fourier transform IR spectroscopy: in vivo toxicity of carbon tetrachloride on rat liver. *Biopolymers* 57: 160-168, 2000.

30. Neaud V, Gillibert Duplantier J, Mazzocco C, Kisiel W, and Rosenbaum J. Thrombin Up-regulates Tissue Factor Pathway Inhibitor-2 Synthesis through a Cyclooxygenase-2-dependent, Epidermal Growth Factor Receptor-independent Mechanism. *J Biol Chem* 279: 5200-5206, 2004.

31. **Neubauer K, Knittel T, Armbrust T, and Ramadori G.** Accumulation and cellular localization of fibrinogen/fibrin during short-term and long-term rat liver injury. *Gastroenterology* 108: 1124-1135, 1995.

32. **Recknagel RO, Glende EA, Jr., Dolak JA, and Waller RL.** Mechanisms of carbon tetrachloride toxicity. *Pharmacol Ther* 43: 139-154, 1989.

33. **Riewald M and Ruf W.** Protease-activated receptor-1 signaling by activated protein C in cytokine-perturbed endothelial cells is distinct from thrombin signaling. *J Biol Chem* 280: 19808-19814, 2005.

34. Rullier A, Senant N, Kisiel W, Bioulac-Sage P, Balabaud C, Le Bail B, and Rosenbaum J. Expression of protease-activated receptors and tissue factor in human liver. *Virchows Arch*: 1-6, 2005.

35. Safadi R, Ohta M, Alvarez CE, Fiel MI, Bansal M, Mehal WZ, and Friedman SL. Immune stimulation of hepatic fibrogenesis by CD8 cells and attenuation by transgenic interleukin-10 from hepatocytes. *Gastroenterology* 127: 870-882, 2004.

36. Tuchweber B, Desmoulière A, Bochaton-Piallat ML, Rubbia-Brandt L, and Gabbiani G. Proliferation and phenotypic modulation of portal fibroblasts in the early stages of cholestatic fibrosis in the rat. *Lab Invest* 74: 265-278, 1996.

37. Wanless IR, Liu JJ, and Butany J. Role of thrombosis in the pathogenesis of congestive hepatic fibrosis (cardiac cirrhosis). *Hepatology* 21: 1232-1237, 1995.

Figure 1 : Effect of an acute CCl₄ treatment on liver microsome peroxidation

Microsomal fractions of liver from mice acutely treated with CCl₄ were analyzed by FT-IR spectroscopy as described in Materials and Methods. Results are shown as a dendrogram representing liver peroxidation as assessed by FT-IR spectroscopy (1130-930 cm⁻¹ spectral interval, which mainly contains glycogen). All samples from CCl₄-treated mice (n = 15), whether PAR-1^{+/+}, PAR-1^{+/-}, or PAR-1^{-/-} clustered together on the left side (clusters 1-8) whereas all control samples (n = 15, clusters 9-11) clustered separately on the right side. Spectra in clusters 9-11 present significant molecular content differences (H values = heterogeneity) from those of the 1-8 series (*: P < 0.01).

Figure 2 : Effect of PAR-1 deficiency on fibrosis deposition.

Fibrosis was stained with picrosirius red and the staining was quantified by histomorphometry.

a : controls; b-d : mice treated for 6 weeks with CCl₄ (b: PAR-1^{+/+}; c : PAR-1^{+/-}; d : PAR-1^{-/-}) (picrosirius red ; x10) ; e: The graph shows a box and whiskers plot of percentage of section area occupied by fibrosis. The top and bottom of each box represent the 75th and 25th percentiles, respectively. Whiskers represent the range and the line in the box represents the median value of the distribution. (WT : wild type, HT : heterozygous, KO : knock-out mice for PAR-1 gene). Kruskal-Wallis test showed a significant difference between groups (p < 0.001; n = 15 for PAR-1^{+/+}, PAR-1^{+/-} and PAR-1^{-/-} animals each, and 6 for controls).

Figure 3 : Effect of PAR-1 deficiency on ASMA expression

Fibrogenic cell activation was assessed by staining for ASMA. The area stained positively was quantified by histomorphometry.

a : controls; b-d : mice treated for 6 weeks with CCl₄ (b: PAR-1^{+/+}; c : PAR-1^{+/-}; d : PAR-1^{-/-}) (immunostaining ASMA ; x20) ; e : the graph shows a box and whiskers plot of percentage of section area occupied by ASMA-positive cells. The top and bottom of each box represent the 75th and 25th percentiles, respectively. Whiskers represent the range and the line in the box represents the median value of the distribution. (WT : wild type, HT : heterozygous, KO : knock-out mice for PAR-1 gene) of treatment. Kruskal-Wallis test showed a significant difference between groups (p < 0.001; n = 15 for PAR-1^{+/+}, PAR-1^{+/-} and PAR-1^{-/-} animals each, and 6 for controls).

Figure 4 : Effect of PAR-1 deficiency on the expression of specific transcripts

After 6 weeks of CCl₄, total RNA was extracted from the livers and analyzed by real-time RT-PCR with primers specific for collagen $\alpha 1(I)$ (a), PDGF β -R (b) or MMP-2 (c). Results were normalized using the expression of RLP0 transcripts. The graph shows box and whiskers plots of transcripts levels. The top and bottom of each box represent the 75th and 25th percentiles, respectively. Whiskers represent the range and the line in the box represents the median value of the distribution. P values are shown on the graphs (n = 15 for PAR-1^{+/+}, PAR-1^{+/-} and PAR-1^{-/-} animals each, and 6 for controls); d : western blot for MMP-2 expression in liver extracts of untreated animals (controls), or in WT or PAR-1^{-/-} animals that received CCl₄.

Figure 5: Hypoxia labeling in the mice liver after 6 weeks of treatment

Mice were injected with pimonidazole before sacrifice and liver sections were stained with the Hypoxyprobe 1-Mab-1 as described in Materials and Methods. a: control; b-d : mice treated with CCl_4 for 6 weeks (b : PAR-1^{+/+}; c: PAR-1^{+/-}; d: PAR-1^{-/-}). The continuous sinusoidal staining seen in all pictures was also seen in sections obtained from mice not

injected with pimonidazole (not shown) and was thus considered non specific. e : the graph shows a box and whiskers plot of the number of hypoxia-positive cells counted in 12 non overlapping fields. The top and bottom of each box represent the 75th and 25th percentiles, respectively. Whiskers represent the range and the line in the box represents the median value of the distribution. (WT : wild type, HT : heterozygous, KO : knock-out mice for PAR-1 gene) of treatment. Kruskal-Wallis test showed a significant difference between groups (p < 0.001; n = 15 for PAR-1^{+/+}, PAR-1^{+/-} and PAR-1^{-/-} animals each, and 6 for controls).

Figure 6: CD3-positive cells in the mice liver after 6 weeks of treatment

CD3-positive cells were labeled as described in Materials and Methods. a: control; b-d : mice treated with CCl₄ for 6 weeks. Numerous positive cells were observed in PAR-1^{+/+} mice treated for 6 weeks with CCl₄ (b, arrows). The number of CD-3 positive cells was reduced in PAR-1^{+/-} mice (c) and even more in PAR-1^{-/-} mice (d). e : the graph shows a box and whiskers plot of the number of CD3-positive cells counted in 12 non overlapping fields. The top and bottom of each box represent the 75th and 25th percentiles, respectively. Whiskers represent the range and the line in the box represents the median value of the distribution. (WT : wild type, HT : heterozygous, KO : knock-out mice for PAR-1 gene) of treatment. Kruskal-Wallis test showed a significant difference between groups (p < 0.001; n = 15 for PAR-1^{+/+}, PAR-1^{+/-} and PAR-1^{-/-} animals each, and 6 for controls).

| Name | Primer sequence | Amplicon size (bp) |
|------------------------|---|--------------------|
| RLP0 | F 5'GGC GAC CTG GAA GTC CAA CT 3' | 149 |
| | R 5' CCA TCA GCA CCA CAG CCT TC 3' | |
| Collagen $\alpha 1(I)$ | F 5' ATG TTC AGC TTT GTG GAC CT 3' | 92 |
| | R 5' CAG CTG ACT TCA GGG ATG T 3' | |
| MMP2 | F 5' CTG CGC TTT TCT CGA ATC CA 3' | 81 |
| | R 5' GGG TAT CCA TCT CCA TGC TCC 3' | |
| PDGFβ receptor | F 5' TTC CAG GAG TGA TAC CAG CTT 3' | 104 |
| | R 5' AGG GGG CGT GAT GAC TAG G 3' | |
| MCP-1 | F 5' TTC TGG GCC TGC TGT TCA C 3' | 158 |
| | R 3' ACA CCT GCT GCT GGT GAT C 3' | |
| CTGF | F 5' CCC TAG CTG CCT ACC GAC T 3' | 113 |
| | R 5' CAT TCC ACA GGT CTT AGA ACA GG 3' | |
| PAR-1 | F 5' AGC CTT CCT CTG AAC GTC CT 3' | 149 |
| | R 5' CCG GAG AAG TAG TAG CTG ATC 3'T | |

Table 1 : Primer sequences used for real-time quantitative RT-PCR

RLP0 : human acidic ribosomal phosphoprotein P0 ; PAR-1/ protease activated receptor-1; MMP2 : matrix metalloprotease 2 ; PDGF β : Platelet Derived Growth Factor β ; MCP-1 : monocyte chemotactic protein-1; CTGF : connective tissue growth factor; F : forward ; R : reverse.

| Table 2 : CCl ₄ -acute liver toxicity : aminotransferase levels and centrolobular necrosis |
|---|
| in the three groups |

| | PAR-1 ^{+/+} | PAR-1 ^{+/-} | PAR-1-/- | р |
|------------------------|-----------------------------|----------------------|----------------|----|
| ASAT (IU/l) | 1002 (981- | 2217 (1176- | 1423 (963- | ns |
| | 1023) | 3258) | 2976) | |
| ALAT (IU/l) | 2379 (1443- | 4394 (2047- | 3916 (3333- | ns |
| | 3315) | 6741) | 6564) | |
| Centrolobular necrosis | 24.25 (22.5- | 32 (22.8-35) | 29.5 (27-29.7) | ns |
| (% of section area) | 32) | | | |

| | controls | PAR-1 ^{+/+} | PAR-1 ^{+/-} | PAR-1 ^{-/-} | р |
|-------------------|-------------------|----------------------|----------------------|----------------------|--------|
| Body weight (g) | 34.10 (32.2-37.7) | 33.5 (27.4-36.3) | 33.1 (28.9-39.4) | 32.45 (27.6-37.6) | ns |
| Spleen weight (g) | 0.089 (0.07-0.13) | 0.115 (0.07-0.16) | 0.103 (0.07-0.13) | 0.108 (0.07-0.16) | ns |
| Liver weight (g) | 1.1 (0.8-1.4) | 1.4 (1-1.6) | 1.4 (1-1.8) | 1.4 (0.6-1.8) | 0.05 |
| Liver w/body w | 0.03 (0.02-0.03) | 0.04 (0.02-0.05) | 0.04 (0.02-0.04) | 0.04 (0.02-0.05) | < 0.01 |
| ASAT (IU/l) | 194.5 (151-223) | 279 (183-435) | 290 (186-789) | 285.5 (125-487) | ns |
| ALAT (IU/l) | 29.5 (21-39) | 82 (59-123) | 85 (50-151) | 87.5 (56-143) | 0.01 |

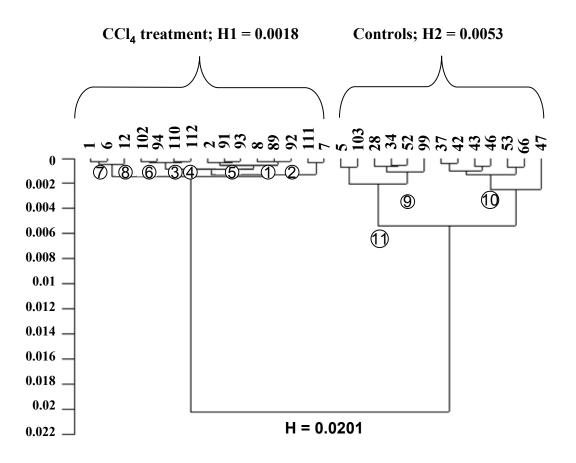
Table 3: Vital parameters and liver function tests in mice after 6 weeks of CCl₄ treatment

28

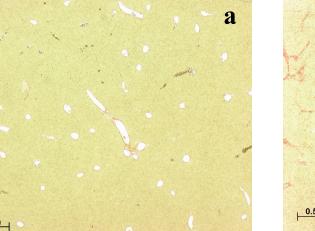
| | Controls | PAR-1 ^{+/+} | PAR-1 ^{+/-} | PAR-1-/- |
|-------|---------------|----------------------|----------------------|-----------------|
| CTGF | 6.6 (1.0-8.9) | 16.7 (5.2-37.0) | 15.1 (3.0-67.2) | 11.3 (3.1-32.2) |
| MCP-1 | 3.2 (1.0-7.3) | 7.2 (2.8-17.8) | 5.1 (1.2-27.1) | 4.9 (1.7-11.4) |

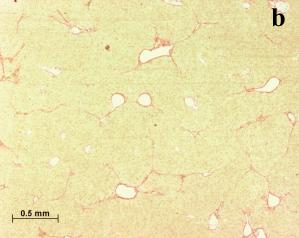
Table 4 : Expression of CTGF and MCP-1 transcripts

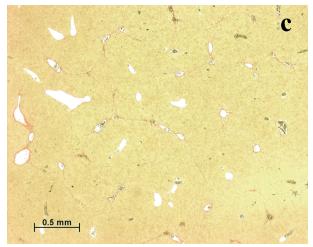
The values are the median (range) of gene expression results normalized to RLP0 (n = 12 for PAR-1^{+/+}, PAR-1^{+/-} and PAR-1^{-/-} animals each, and 5 for controls). The differences did not reach statistical significance.

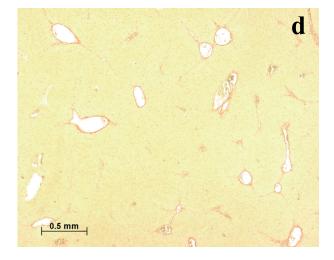


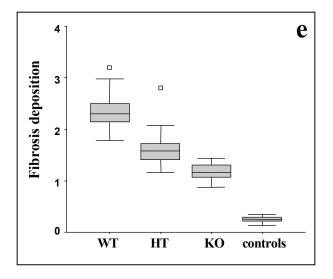


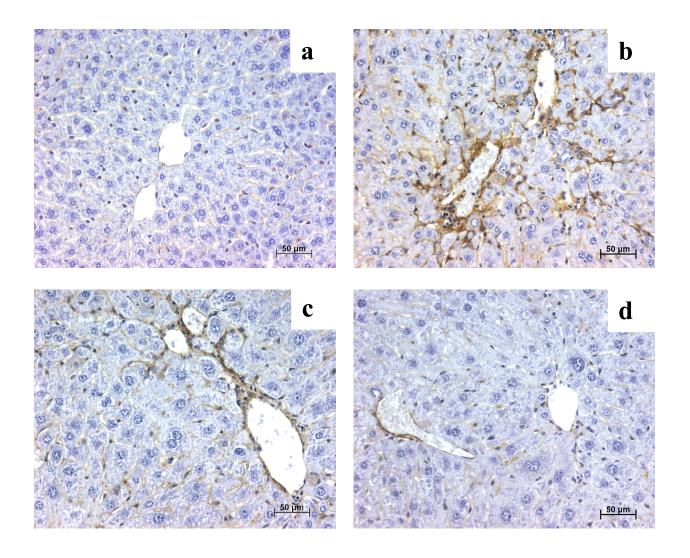


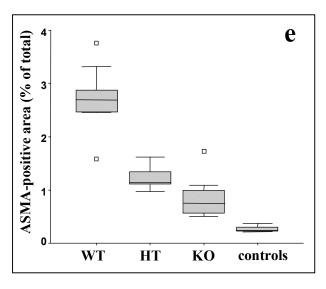




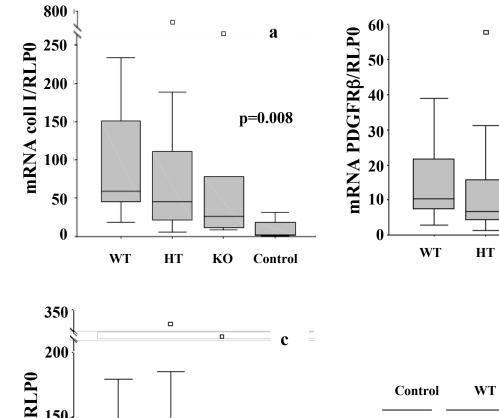


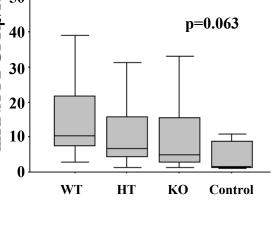












d

b

